Original paper

Perryite, $(Ni,Fe)_{16}PSi_5$, from the Mount Egerton aubrite: the first natural P–Si-ordered phosphide-silicide

Sergey N. BRITVIN[1,2*], Sergey V. KRIVOVICHEV[2,1], Oleg S. VERESHCHAGIN[1], Natalia S. VLASENKO[1], Vladimir V. SHILOVSKIKH[1], Maria G. KRZHIZHANOVSKAYA[1], Maksim S. LOZHKIN[1], Edita V. OBOLONSKAYA[3], Yulia O. KOPYLOVA[1]

[1] *Saint Petersburg State University, Universitetskaya Nab. 7/9, 199034, St. Petersburg, Russia; sergei.britvin@spbu.ru*
[2] *Kola Science Center, Russian Academy of Sciences, Fersman Str. 14, 184209, Apatity, Russia*
[3] *The Mining Museum, Saint Petersburg Mining University, 21st Line 2, 199106, St. Petersburg, Russia*
[*] *Corresponding author*

Perryite, natural Ni-silicide, is a minor but regular constituent of the metal phase in enstatite chondrite (aubrite) and enstatite chondrite meteorites. Its synthetic analog was shown to have promising catalytic properties. The first-time solution of the crystal structure of natural perryite was completed on the material from the Mount Egerton aubrite. The mineral is trigonal, $R\bar{3}c$, a = 6.6525(5), c = 37.998(5) Å, V = 1456.3(3) and Z = 6. The structure was refined to R_1 = 0.0137 based on 457 independent observed reflections. The chemical formula obtained from the structure refinement, $(Ni_{14.14}Fe_{1.88})_{\Sigma 16.02}PSi_5$, agrees with that derived from the electron microprobe data, $(Ni_{13.39}Fe_{2.65}Co_{0.01})_{\Sigma 16.05}P_{1.22}Si_{4.74}$. This research showed that P and Si in perryite are ordered, resulting in the simplified formula $(Ni,Fe)_{16}PSi_8$, in contrast to the currently accepted variant $(Ni,Fe)_8(Si,P)_3$. The detailed results of EBSD study reveal previously unknown relationships between perryite, associated α-(Fe,Ni) metal (also known as *kamacite*) and schreibersite, $(Fe,Ni)_3P$. Since enstatitic meteorites represent the early stages of nebular accretion, our results demonstrate that the crystal-chemical factor could affect the differentiation of chemical elements upon the onset of the Solar System formation.

Keywords: silicide, phosphide, aubrite, enstatite chondrite, meteorite, crystal structure
Received: 7 July 2021; accepted: 10 November 2021; handling editor: F. Laufek
The online version of this article (doi: 10.3190/jgeosci.331) contains supplementary electronic material.

1. Introduction

Perryite is the first metal silicide discovered in nature. Originally reported in the anomalous iron of the Horse Creek meteorite (Fredriksson and Henderson 1965), it was shortly afterward described from enstatite chondrites Kota-Kota and South Oman (Reed 1968), followed by the identification in the aubrites (enstatite achondrites) Mount Egerton and Norton County (Wai 1970). The mineral is now recognized as a common, albeit subordinate, a constituent of the metal phase in aubrites and in type 3–4 enstatite chondrites (Tab. 1). Silicon-rich α-(Fe,Ni) metal in these meteorites is considered a primary phase crystallized on the initial stages of protoplanetary nebula condensation. Perryite, being always confined to Si-rich kamacite, was a subject of studies devoted to the formation of asteroidal bodies (Wasson and Wai 1970; Casanova et al.1993; Kimura and Lin 1999).

Synthetic $(Ni,Fe)_8(Si,P)_3$, having a stoichiometry close to that of perryite, was structurally characterized by Okada et al. (1991). The authors show topological similarity between $(Ni,Fe)_8(Si,P)_3$ and $Ni_{31}Si_{12}$ (Frank and Schubert 1971). The absence of Ni_8Si_3 in the Ni–Si phase diagram (Ellner et al. 1979) evidences that Ni/Fe and Si/P substitutions may play an essential role in stabilizing the crystal structure of $(Ni,Fe)_8(Si,P)_3$ (Okada et al. 1991). Marsh (1994) re-examined the data by Okada et al. (1991) and noticed that there are strong indications that P can be selectively incorporated into the Si(3) site. Yang et al. (2015) reported on the results of the high-pressure study of synthetic perryite analog. Recently, Zhang et al. (2021) conducted the research of electrocatalytic properties of synthetic perryite analog and its Ge-substituted counterparts. However, as far as we know, crystallographic studies on natural perryite have never been performed. The lack of crystallographic information and the ambiguity of chemical data on natural perryite inspired us to study this mineral, using the material from the Mount Egerton meteorite. We herein present crystal-structure evidence for the P–Si ordering in natural perryite and describe its crystallographic relationships with associated minerals – α-(Fe,Ni) metal and schreibersite.

2. The Mount Egerton aubrite

A few fragments of this meteorite were collected in 1941 along the headstream of the Gascoine River,

Tab. 1 Formula coefficients in perryite from enstatitic meteorites.

	N [a]	Formula coefficients based on 22 atoms per formula unit						Ref. [b]
		Ni	Fe	Minor	Si	P	Ni+P	
Aubrites								
Mount Egerton	18	14.32	1.78		4.69	1.21	5.90	[1]
	6	13.74	2.46		4.82	0.97	5.80	[2]
Norton County	25	15.48	0.60		4.06	1.86	5.92	[1]
	1	15.69	0.37	Co 0.02	4.39	1.53	5.92	[3]
	1	15.40	0.78		4.29	1.53	5.82	[3]
	9	15.36	0.78		4.34	1.51	5.85	[2]
	6	15.61	0.22	Cu 0.06	5.15	0.97	6.12	[4]
Horse Creek	1	15.01	0.58		4.65	1.76	6.40	[5]
	1	15.00	0.80		4.76	1.44	6.20	[6]
	1	15.06	0.79	Co 0.01	4.69	1.45	6.15	[7]
Enstatite chondrites								
ALH 77156 (EH3-4)	1	15.29	0.65	Cu 0.04	4.83	1.18	6.02	[8]
Kaidun III (EH)	1	13.05	2.55	Co 0.02	5.12	1.26	6.37	[9]
Kota-Kota (EH3)	1	15.13	0.79		4.84	1.24	6.08	[6]
	1	15.17	0.90		4.72	1.20	5.93	[10]
MAC 88136 (EL3)	13	14.88	1.03	Cu 0.01	4.17	1.91	6.08	[11]
Parsa (EH3-5)	1	15.10	1.00		4.66	1.24	5.90	[12]
Qingzhen (EH3)	1	14.13	1.79		4.96	1.11	6.07	[13]
	1	14.50	1.67	Cr 0.02	4.59	1.22	5.81	[14]
	111	14.71	1.12	Cu 0.07	4.90	1.20	6.10	[11]
South Oman (EH3)	1	14.07	1.23		5.84	0.85	6.69	[6]
Yamato 74370 (EH3)	1	15.10	0.99		4.73	1.18	5.91	[15]

[a] *N* – number of analytical points.
[b] References: [1] Wasson and Wai (1970); [2] Casanova et al. (1993); [3] Okada et al. (1988); [4] Garvie et al. (2021); [5] Fredriksson and Henderson (1965); [6] Reed (1968); [7] Wai (1970); [8] Kimura and Lin (1999); [9] Grokhovskii and Ivanov (1986); [10] Prinz et al. (1984); [11] Lin and El Goresy (2002); [12] Nehru et al. (1984); [13] Rambaldi and Rajan (1983); [14] Lee et al. (1995); [15] Nagahara and El Goresy (1984).

ca. 12 miles to the north of Mount Egerton, 24°46'01.2"S 117°42'00.0"E, Victoria, Australia (McCall 1965). The larger pieces of the meteorite (up to 77 g) were predominantly composed of centimeter-sized enstatite crystals, whereas the smaller ones comprised Fe–Ni metal enriched in silicon (McCall 1965). Later efforts of meteorite collectors have brought thousands of Mount Egerton enstatite specimens available worldwide, but nothing of the metal fragments, which seem to have been entirely harvested during the first findings. The Mount Egerton meteorite is now classified as an anomalous aubrite (enstatite achondrite) (Meteoritical Bulletin Database). Its specific feature is a lack of brecciation of enstatite fragments typical for the majority of aubrites. The unusual structure of its metal, like that of the Horse Creek iron (McCall 1965), appears to be due to a network of perryite lamellae (Wai 1970; Wasson and Wai 1970).

3. Samples and methods

All analytical procedures were carried out using the equipment and software provided by the Scientific Park of St. Petersburg State University. A ca. 0.5 × 1 cm^2 fragment of the Mount Egerton aubrite, consisting of an intergrowth of α-(Fe,Ni) metal and schreibersite with inclusion of enstatite, was generously provided for this study by the curators of the Mining Museum, St. Petersburg Mining University (a part of the specimen MM280). The piece was cut into two halves, which were polished, gently etched with nital, coated with carbon film and subjected to electron microprobe investigation. The latter was carried out employing a Hitachi S-3400N SEM equipped with an INCA WAVE 500 WDX spectrometer operated at 20 kV and 15 nA. Elemental Ni, Co, Fe and Si, along with natural schreibersite (for P), were used as analytical standards ($K\alpha_1$ series lines). Electron backscatter diffraction (EBSD) study was performed on the section preliminary etched with Ar-ion beam using an Oxford Instruments IonFab-300 system (500 V, 2.4 mA cm^{-2}, 20 min treatment time). EBSD phase identification and mapping were carried out with an Oxford Instruments Nordlys-HKL EBSD detector operated at 30 kV and 1.5 nA, both in spot and mapping modes. The sample was coated with ~2 nm carbon film and glued with carbon tape onto a 70° tilted stage. For identification, averaging of 20 patterns with no binning was performed; averaging of 2 patterns and 2 × 2 binning were utilized during mapping. The original authors' crystallographic data on perryite, schreibersite and kamacite were used for the

EBSD matching. The smaller slice of kamacite was dissolved in a warm 10 % HCl. After complete removal of α-(Fe,Ni) metal, rinsing the residue with methanol and air-drying on the clock glass, a shiny layer composed of platy perryite lamellae was obtained. Powder X-ray diffraction pattern was recorded from a few lamellae randomly glued onto a glass fiber. A Rigaku RAXIS Rapid II diffractometer was used in the following setup: Co$K\alpha$ radiation (rotating anode, 40 kV, 15 mA), microfocus mirror monochromator, semi-cylindrical imaging plate (r = 127.4 mm, $2\theta_{max}$ = 140°), Debye-Scherrer geometry, Gandolfi-type sample rotation, exposure 30 min. The raw data were converted into XY profile using osc2xrd program (Britvin et al. 2017). Pattern indexing and unit-cell refinement were performed with Bruker TOPAS 5.0 software (Bruker Inc., Massachusetts, USA). A single-crystal study was carried out on the non-twinned crystal by means of a Bruker Kappa APEX DUO diffractometer (MoK_α, 50 kV, 0.6 mA, microfocus tube with a mirror monochromator, 1024K CCD detector). The collected data were processed using Bruker APEX2 software (Bruker Inc., Massachusetts, USA). The crystal structure was solved and refined to R_1 = 0.0128 using *SHELX*-2018 program suite (Sheldrick 2015) incorporated into Olex2 GUI shell (Dolomanov et al. 2009). Further details on single-crystal data acquisition, integration and structure refinement can be retrieved from the CIF file included in Supplementary material.

4. Results

4.1. Appearance, general crystallography and chemical composition

Perryite appears as a rectangular grid of thin lamellae penetrating α-(Fe,Ni) metal matrix (Fig. 1a, b). The mineral has a yellowish-creamy color in reflected light, possesses a distinct pleochroism in creamy hues and is weakly anisotropic. Individual perryite lamella can reach 10 μm in width, whereas interlamellar grid spacing varies from 30 to 100 μm. EBSD mapping reveals that the host α-(Fe,Ni) metal forms an entire single crystal, whereas perryite lamella are composed of platy sub-domains filling up octahedral cleavage interstices in the metal (Fig. 1c, 2). The difference between the rectangular perryite-metal pattern shown in Fig. 1 and a pseudo-Widmanstätten octahedral structure described by Wai (1970) is likely caused by the different orientation of α-(Fe,Ni) metal cuts. In our case, the {111} plane of the host metal crystal is inclined by ~13° relative to the cut plane (Fig. 2d). An X-ray single-crystal study shows that perryite lamellae are flattened on {001}. EBSD orientation mapping documented that the metal cleavage

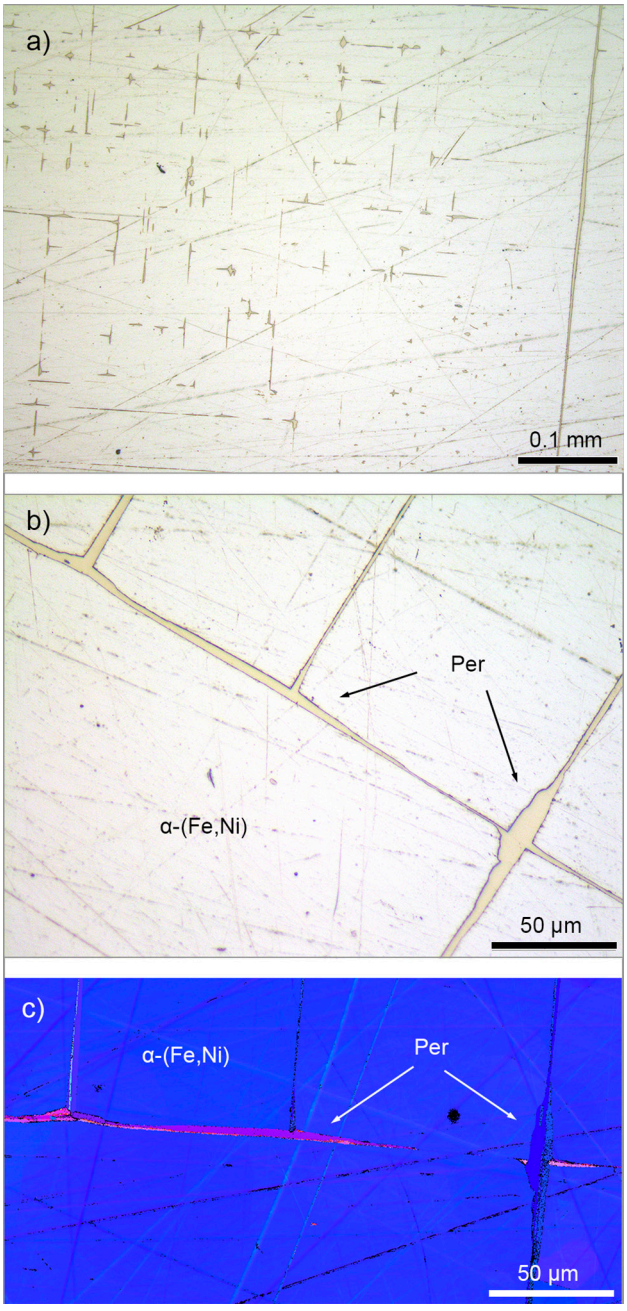

Fig. 1 Perryite in the Mount Egerton aubrite. **a** – Orthogonal grid of perryite lamellae penetrating α-(Fe,Ni) metal matrix. Polished section etched with nital. Reflected light. **b** – A close-up view of perryite lamella. **c** – EBSD orientation map in inverse pole figure color scheme (hereinafter is IPF map) of the same area rotated counterclockwise, projection along the Z-axis. α-(Fe,Ni) forms a single crystal which is cut approximately parallel to {111}. Perryite appears as polycrystalline fillings along octahedral cleavage planes of the host metal. Abbreviation: Per – perryite.

planes are filled with three-component interpenetration twins (trillings) of perryite, formed by rotation of twin domains by 120° around the **c** axis (Fig. 2). The interphase orientation at the perryite-metal interface can be described as {001} perryite = {111} metal. A ~2 × 1 mm

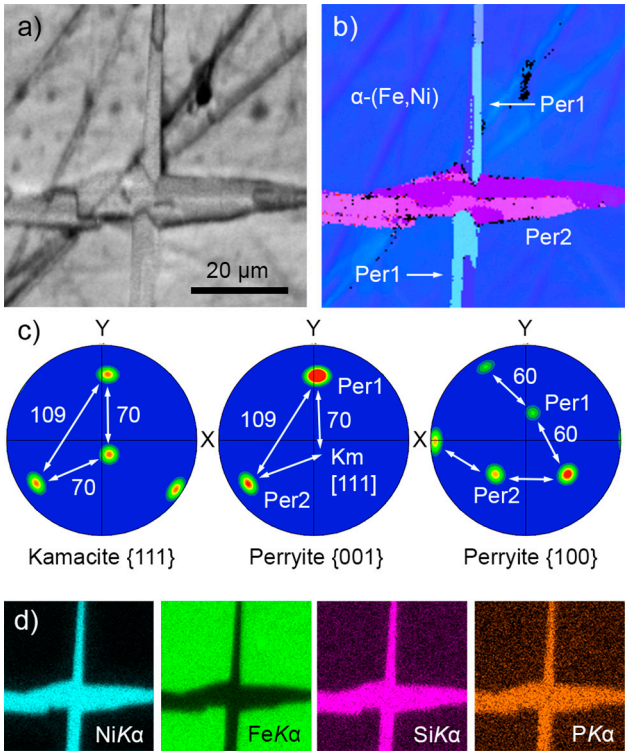

Fig. 2 A close-up view of two crossed perryite lamella in the metal matrix. **a** – EBSD band contrast image highlights interlamellar junctions. **b** – EBSD IPF map of the same area, view along the Z-axis. **c** – EBSD inverse pole figures of α-(Fe,Ni) and perryite (interpole angles in degrees). The {111} plane of α-(Fe,Ni) crystal is inclined by ~13° relative to the image plane. The [001] poles of both perryite lamella subsets, Per1 and Per2, are coincident with the [111] poles of α-(Fe,Ni). Perryite projection onto {100} shows two sets of pole figures corresponding to Per1 and Per2 subsets. Each of the subsets, in due course, represents a 3-component twin (trilling) formed by 120° rotation around [001] axis. **d** – Elemental maps in characteristic X-rays of corresponding elements. Abbreviation: Per – perryite.

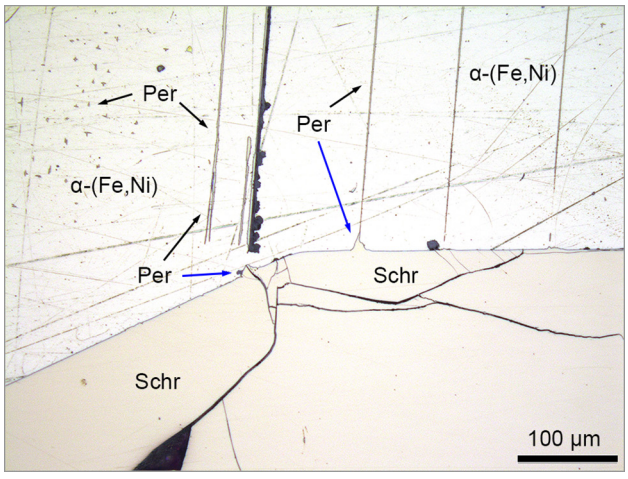

Fig. 3 – A series of perryite lamella abut schreibersite crystal, forming dilation joints (marked by blue arrows) at the metal-schreibersite boundary. Polished section etched with nital. Reflected light. Abbreviations: Per – perryite; Schr – schreibersite.

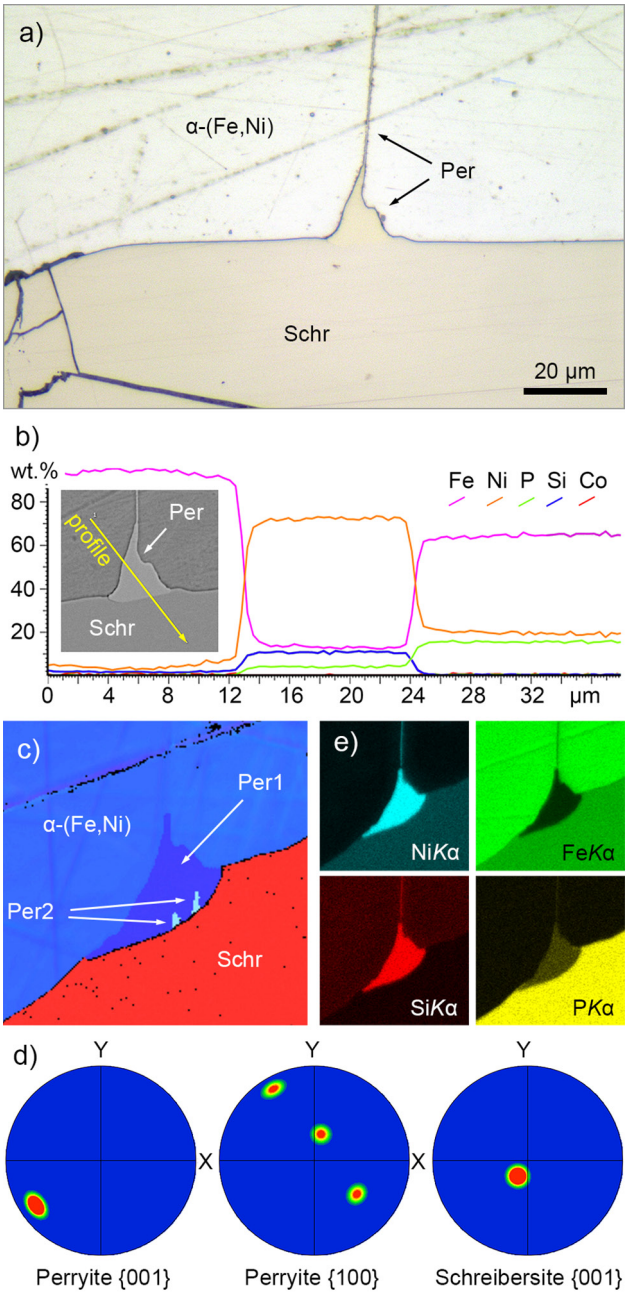

Fig. 4 Dilation joint of perryite lamella at the metal-schreibersite interface. **a** – Polished section after nital etch, view in reflected light. **b** – Elemental profile across the metal-perryite-schreibersite junction. **c** – EBSD IPF map, view along the **Z**-axis. Note that both α-(Fe,Ni) and schreibersite form single crystals, whereas perryite droplet consists of two orientation domains denoted as Per1 and Per2. **d** – Inverse pole figures related to perryite and α-(Fe,Ni). Note that [001] and [100] poles of Per1 and Per2 domains are geometrically coincident, indicative for the rotational twin around [001] axis. The {001} plane of schreibersite crystal is inclined by ~15° from the image plane. **e** – Elemental maps of the same area in characteristic X-rays of corresponding elements. Abbreviations as in Fig. 3.

long, single-crystal schreibersite grain is cut approximately on {001} on the contact with the metal (Fig. 3). At every point where perryite lamellae abut schreibersite,

one can observe peculiar delta-shaped dilation joints (Figs 3, 4). They are filled entirely with perryite and partially sink into schreibersite matrix, reminiscent of liquid droplets (Fig. 4). EBSD mapping of 6 different joints revealed that perryite is polycrystalline, with domain orientations not always coincident with the adjacent lamella.

All three mineral phases constituting the inspected section of Mount Egerton are chemically homogeneous across the entire cut surface (Tabs 2, 3). It is noteworthy that perryite forming a lamellar grid and the mineral filling up dilation joints have precisely the same composition (Tab. 2). Diffusion zones – Ni-rich areas (bands) in the α-(Fe,Ni) metal surrounding perryite (Wai 1970) were not observed in our section of Mount Egerton. The Ni/Fe gradient around perryite was neither detected by EMPA mapping or profiling (Fig. 1c, 2b, 4c) nor by nital etching – the latter would rise to a higher relief of the Ni-rich areas, which was not observed (Fig. 1b, 3, 4a). In this respect, the metal-perryite structures in our specimen are much more similar to the structures of Horse Creek and Norton County than to the previously described sections of Mount Egerton (Wai 1970).

Tab. 2 Chemical composition of perryite in the inspected section of Mount Egerton.

	Lamella cross-sections (N = 11)			Dilation joints (N = 22)		
	wt. %	range	SD	wt. %	range	SD
Ni	70.89	69.13–72.20	1.03	70.18	68.97–71.43	0.63
Fe	13.34	11.62–15.03	1.13	13.56	12.17–14.77	0.78
Co	0.04	0.00–0.21	0.08	0.10	0.00–0.38	0.13
Si	12.01	11.58–12.47	0.27	12.09	11.61–12.47	0.24
P	3.40	3.10–3.85	0.28	3.52	3.28–3.70	0.12
Total	99.68			99.45		
Formula coefficients calculated on 22 atoms per formula unit						
Ni	13.39			13.26		
Fe	2.65			2.69		
Co	0.01			0.02		
Σ	16.05			15.97		
Si	4.74			4.77		
P	1.22			1.26		
Σ	5.96			6.03		

SD – standard deviation

4.2. X-ray powder diffraction and structure refinement

The refinement of unit-cell parameters based on the X-ray powder diffraction pattern (Tab. 4) gave the values of a = 6.672(2), c = 38.055(15) and V = 1467.2(9) Å, consistent with the single-crystal data (Tab. 5) and with previously reported parameters for synthetic perryite analog: a = 6.640(2), c = 37.982(7) and V = 1450.3(7) Å (Okada et al. 1991). The latter shows that natural perryite from Mount Egerton and synthetic $(Ni,Fe)_8(P,Si)_3$ represent the same material. Okada et al. (1991) refined the crystal structure of $(Ni,Fe)_8(Si,P)_3$

Tab. 3 Chemical composition of α-(Fe,Ni) metal and schreibersite.

	α-(Fe,Ni) (N = 8)			Schreibersite (N = 6)		
	wt. %	range	SD	wt. %	range	SD
Fe	93.49	92.31–94.33	0.68	66.82	65.52–68.09	0.99
Ni	3.35	2.56–4.59	0.61	17.36	16.07–18.58	1.08
Co	0.45	0.37–0.52	0.05	0.17	0.15–0.19	0.01
Si	2.17	2.02–2.29	0.10	0.23	0.18–0.28	0.04
P	<0.10			15.49	15.20–15.69	0.17
Total	99.46			100.07		

SD – standard deviation

Tab. 4 X-ray powder diffraction data for perryite from the Mount Egerton aubrite (d in Å).

$I_{meas.}$	$d_{meas.}$	$I_{calc.}$	$d_{calc.}$	*hkl*	$I_{meas.}$	$d_{meas.}$	$I_{calc.}$	$d_{calc.}$	*hkl*
3	3.346	>1	3.336	110	10	1.702	15	1.703	1.2.14
3	3.176	1	3.178	1.0.10	3	1.656	2	1.657	1.0.22
		2	3.171	0.0.12	2	1.586	2	1.586	0.0.24
8	2.952	6	2.953	116	2	1.423	3	1.424	0.3.18
8	2.766	5	2.764	024			3	1.424	3.0.18
14	2.620	11	2.619	119	4	1.393	8	1.394	2.2.15
11	2.465	7	2.469	208	2	1.309	4	1.310	2.2.18
13	2.300	10	2.301	0.2.10	4	1.268	5	1.268	0.0.30
22	2.180	23	2.180	211	1	1.251	3	1.252	3.2.10
11	2.127	12	2.129	214	2	1.248	3	1.249	2.1.25
11	2.115	7	2.114	0.0.18	3	1.191	9	1.191	2.3.14
8	2.100	10	2.099	125	1	1.186	3	1.186	1.1.30
100	2.019	100	2.019	1.1.15	2	1.128	3	1.129	1.4.15
27	1.980	10	1.985	128			3	1.129	4.1.15
		21	1.980	2.0.14	3	1.082	8	1.081	1.4.18
62	1.925	84	1.926	300			8	1.081	4.1.18
4	1.893	5	1.894	2.1.10	3	1.059	2	1.059	3.0.30
4	1.845	5	1.847	1.2.11	2	1.044	5	1.044	1.2.32
11	1.786	14	1.786	1.1.18					

Tab. 5 Crystal parameters, data collection and structure refinement details for natural perryite.

Crystal Data	
Formula	$(Ni_{14.14}Fe_{1.88})_{\Sigma 16.02}PSi_5$
Crystal size (mm)	0.04 × 0.03 × 0.005
Crystal system, space group	Trigonal, $R\bar{3}c$
a, *c* (Å)	6.6525(5), 37.998(5)
V (Å^3)	1456.3(3)
Z	6
D_x (g cm^{-3})	7.563
Data collection and refinement	
Radiation	Mo*K*α (λ = 0.71073 Å)
Temperature (*K*)	296
2θ max (°)	truncated at 60.00
F(000)	3175.6
μ (mm^{-1})	30.10
No. of measured, independent and observed [$I > 2\sigma(I)$] reflections	4383, 481, 457
No. of parameters	38
Average $I/\sigma(I)$	58
h, k, l range	–9→9, –9→9, –52→51
Data completeness	0.998
$R_{int.}$, R_σ	0.0278, 0.0171
R_1 [$F \geq 4\sigma(F)$], R_1 (all data)	0.0137, 0.0128
wR_2	0.0296
GooF	1.058
Residual density (e Å^{-3}) (min, max)	–0.64, 0.83

in the non-centrosymmetric space group *R*3*c*. Marsh (1994) re-refined the structure based on the original data by Okada et al. (1991) and showed that the refinement in $R\bar{3}c$ gives somewhat better results. Today, inversion center recognition's reliability can be assessed numerically (Flack and Bernardinelli 2008). The chemical composition of perryite, allows discrimination between $R\bar{3}c$ and *R*3*c* based on the data collected with MoK_α radiation. In the case of the mineral from Mount Egerton, both reflection statistics and comparison of structure refinements unequivocally indicate the space group $R\bar{3}c$. The latter implies the occurrence of 7 independent structural sites: 4 (Ni,Fe) and 3 positions which can be populated by Si and P (Tab. 6). The similarity of atomic scatterers within the pairs Fe/Ni (*Z* = 26/28) and Si/P (*Z* = 14/15) makes the reliable refinement of their populations a challenging task. However, it was recently shown that such refinements succeed upon compliance with the following conditions: (1) High brightness of reflections dataset; (2) High redundancy and (3) 2θ limit allowing the achievement of data-to-parameter ratio > 8 (Britvin et al. 2021). The refinement of the perryite structure resulted in a successful determination of site populations (expressed as structural occupational factor, *s.o.f.*). We found that *M*1, *M*2 and *M*4 sites are Ni-dominant, whereas *M*3 site is completely occupied by Ni. The free refinements of non-metal sites evidence with high fidelity (*e.s.d.s.* ≤ 0.005 *s.o.f.*) that *X*1 and *X*2 positions are occupied solely by Si, whereas *X*3 site is populated by P (Tab. 6). Consequently, the final refinement was carried out with the occupancies of *M*3 and non-metal sites fixed at unity. The chemical formula obtained from the structure refinement $(Ni_{14.14}Fe_{1.88})_{\Sigma 16.02}PSi_5$, agrees well with the empirical formula derived from the electron microprobe data, $(Ni_{13.39}Fe_{2.65}Co_{0.01})_{\Sigma 16.05}P_{1.22}Si_{4.74}$. The insignificant deviations of P and Si contents from the integer values in the empirical formula may be accounted for the limited substitution of Si for P (less than 5 rel. %).

4.3. Crystal structure

Perryite has a layered crystal structure similar to the structures of synthetic silicide $Ni_{31}Si_{12}$ (space group *P*321) and phosphide α-Ni_8P_3 (*R*3c) (Frank and Schubert 1971; Il'nitskaya et al. 1987; Okada et al. 1991). As it is quite common among phosphides and silicides, coordination polyhedra of (Ni,Fe) in perryite are non-convex and very complex. The metal atoms are cross-coordinated by themselves, by each other and by phosphorus atoms (Tab. 7). In contrast, P and Si are coordinated by metal atoms only and form simpler polyhedra (Fig. 5). Therefore, we herein describe the structure

Tab. 6 Fractional atomic coordinates, isotropic displacement parameters and site populations (Å^2) for natural perryite.

Site	*x/a*	*y/b*	*z/c*	U_{iso}	Population	*apfu*
*M*1 (36*f*)	0.33087(3)	0.41408(4)	0.05214(2)	0.01257(9)	Ni 0.86(2) [a]	5.16
*M*2 (36*f*)	0.33718(3)	0.03305(3)	0.01764(2)	0.01050(8)	Ni 0.89(2) [a]	5.34
*M*3 (12*c*)	2/3	1/3	0.05193(2)	0.01095(11)	Ni 1 [1.01(1)] [b]	2.00
*M*4 (12*c*)	0	0	0.06023(2)	0.01126(12)	Ni 0.82(2) [a]	1.64
						Σ 14.14
*X*1 (18*e*)	0.35189(9)	0.01856(9)	0.083333	0.01133(14)	Si 1 [1.002(4)] [b]	3
*X*2 (12*c*)	2/3	1/3	–0.00856(2)	0.00964(15)	Si 1 [0.999(4)] [b]	2
*X*3 (6*b*)	0	0	0	0.01086(19)	P 1 [0.994(5)] [b]	1

[a] The reminder to unity is Fe.

[b] Site occupancy factors were fixed at unity, according to the results of the free refinements given in the brackets.

Tab. 7 Selected interatomic bond-lengths (Å) in natural perryite.[a]

Bond [b]	Length	Bond [b]	Length
*M*1–*M*1^{i}	2.5468(5)	*M*2–*X*1	2.5019(4)
*M*1–*M*2^{ii}	2.6892(5)	*M*2–*X*2^{viii}	2.4491(3)
*M*1–*M*2^{iii}	2.5168(3)	*M*2–*X*2	2.3254(4)
*M*1–*M*2^{iv}	2.5186(3)	*M*2–*X*3	2.2441(2)
*M*1–*M*3	2.5454(3)	*M*3–*M*3^{ix}	2.3866(7)
*M*1–*M*4^{v}	2.6558(4)	*M*3–*X*1^{x}	2.4102(6)
*M*1–*M*4	2.5425(3)	*M*3–*X*1^{iii}	2.4102(6)
*M*1–*X*1^{iii}	2.3112(3)	*M*3–*X*1	2.4102(6)
*M*1–*X*1^{iv}	2.4184(6)	*M*3–*X*2	2.2983(9)
*M*1–*X*2^{vi}	2.3533(6)	*M*4–*X*1^{iv}	2.4447(3)
*M*2–*M*2^{vii}	2.5266(3)	*M*4–*X*1	2.4448(4)
*M*2–*M*2^{ii}	2.5266(3)	*M*4–*X*1^{xi}	2.4447(4)
*M*2–*M*3	2.4726(3)	*M*4–*X*3	2.2887(5)
*M*2–*M*4	2.6844(3)		

[a] Crystallographic tables were created using PublCIF software (Westrip 2010).

[b] Symmetry codes: (i) *x*–*y*+1/3, –*y*+2/3, –*z*+1/6; (ii) *x*–*y*, *x*, –*z*; (iii) –*x*+*y*+1, –*x*+1, *z*; (iv) –*y*, *x*–*y*, *z*; (v) *y*+1/3, *x*+2/3, –*z*+1/6; (vi) –*x*+1, –*y*+1, –*z*; (vii) *y*, –*x*+*y*, –*z*; (viii) –*x*+1, –*y*, –*z*; (ix) *y*+1/3, *x*–1/3, –*z*+1/6; (x) –*y*+1, *x*–*y*, *z*; (xi) –*x*+*y*, –*x*, *z*; (xii) –*x*+1/3, –*x*+*y*–1/3, –*z*+1/6; (xiii) *y*–2/3, *x*–1/3, –*z*+1/6; (xiv) *x*–*y*+1, *x*, –*z*; (xv) *y*+1, –*x*+*y*+1, –*z*; (xvi) –*x*, –*y*, –*z*.

in a phosphorus-centered approach. Phosphorus in perryite is coordinated by 8 metal atoms, forming a distorted cube [PM_8] (Fig. 5a). A similar P-centered cube was found in the structure of α-Ni_8P_3 (Il'nitskaya et al. 1987), whereas all Si atoms in $Ni_{31}Si_{12}$ exhibit higher coordination numbers (Frank and Schubert 1971). Among other Fe-Ni phosphides, a perfect [PNi_8] cube was reported in the structure of nazarovite, $Ni_{12}P_5$, and its synthetic analog (Larsson 1965; Britvin et al. 2022). Polyhedrons [SiM_9] and [SiM_{12}] in perryite are analogous to the P- and Si-centered polyhedra of α-Ni_8P_3 and $Ni_{31}Si_{12}$ (Frank and Schubert 1971; Il'nitskaya et al. 1987). In total, perryite structure can be described as a *c*-axis alternation of the layers belonging to the two different types: (1) The layer composed solely of [$SiNi_{12}$] polyhedra which share common edges and faces, and (2) The layer, which consists of distorted cubes [PM_8] and [$SiNi_{10}$] polyhedra (Fig. 6). The preferential occupancy of the smallest polyhedron (cube) (Tab. 6) by phosphorus rather than silicon looks reasonable from the crystal-chemical point of view.

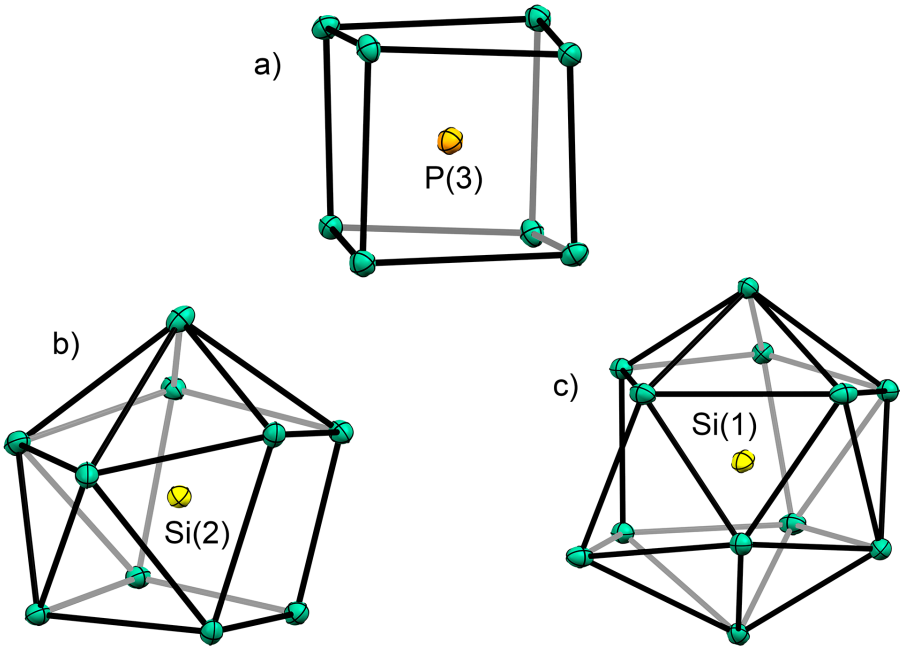

Fig. 5 Phosphorus- and silicon-centered polyhedra in the perryite structure. **a** – Distorted cube [PNi_8]. **b** – Polyhedra [$SiNi_9$] and [$SiNi_{12}$], respectively. Displacement ellipsoids are shown at a 50 % probability level. Drawn with CCDC Mercury 3.8 (Macrae et al. 2006).

5. Discussion

Although Marsh (1994) suggested the possible P-Si ordering in synthetic analogue of perryite, later studies of synthetic material could not resolve this question because of the problems with the proximity of P and Si scattering factors (Zhang et al. 2021). The confirmed Si-P ordering in natural perryite seems to shed light on the absence of "purely silicidic" Ni_8Si_3 in the Ni-Si phase diagram, contrary to the existing silicide $Ni_{31}Si_{12}$. Here the main structural unit is the [PM_8] cube which is an essential part of perryite structure but is absent in the structure of $Ni_{31}Si_{12}$ (Frank and Schubert 1971). Since electron microprobe analyses of perryite from aubrites show the comparable P contents (Tab. 1), one can assume that the structural data obtained on the mineral from Mount Egerton can be reasonably extrapolated on perryite from other enstatite achondrites (Tab. 1). However, the same is not so apparent for enstatite chondrites. Ramdohr (1963) described optically isotropic Ni silicide from enstatite chondrite St. Mark's, which was subsequently ascribed to perryite (Keil 1968). It may appear that the material described from St. Mark's and some other enstatite chondrites (Tab. 1) is a cubic phase similar or identical to a recently described carletonmooreite, Ni_3Si (Barbaro et al. 2021; Garvie et al. 2021). Therefore, further studies are required in order to clarify the nature of Ni-silicide in enstatite chondrites. The results of the present study,

clearly indicating the ordering between P and Si, lead to the new chemical formula of perryite, $(Ni,Fe)_{16}PSi_5$ (Z = 6), which is different from the currently accepted definition, $(Ni,Fe)_8(Si,P)_3$ (Z = 12).

6. Conclusions

We herein demonstrated on the material from enstatite achondrites (aubrites) that crystal-chemical factors could contribute to the differentiation of elements at the earliest stages of Solar System formation. The present research continues the series of works devoted to the ordered solid solutions among natural phosphide minerals (e.g., Skála and Císařová 2005; Drábek 2006; Britvin et al. 2020, 2021) and stimulates further studies in this direction.

Acknowledgments. The authors are indebted to the curators of the St. Petersburg Mining Museum for the specimen of the Mount Egerton aubrite provided for this study. We are grateful to Associate Editor František Laufek for editorial handling of the manuscript. Roman Skála and an anonymous referee made valuable comments and suggestions that substantially improved the quality of the article. This research was completed under the financial support of the Russian Science Foundation, grant 18-17-00079. We thank the resource Centre for X-ray Diffraction Studies, Interdisciplinary Center for Nanomaterials Research, Geomodel and Nanophotonics Resource Centers of SPSU for instrumental and computational support.

Electronic supplementary material. Supplementary crystallographic data for this paper are

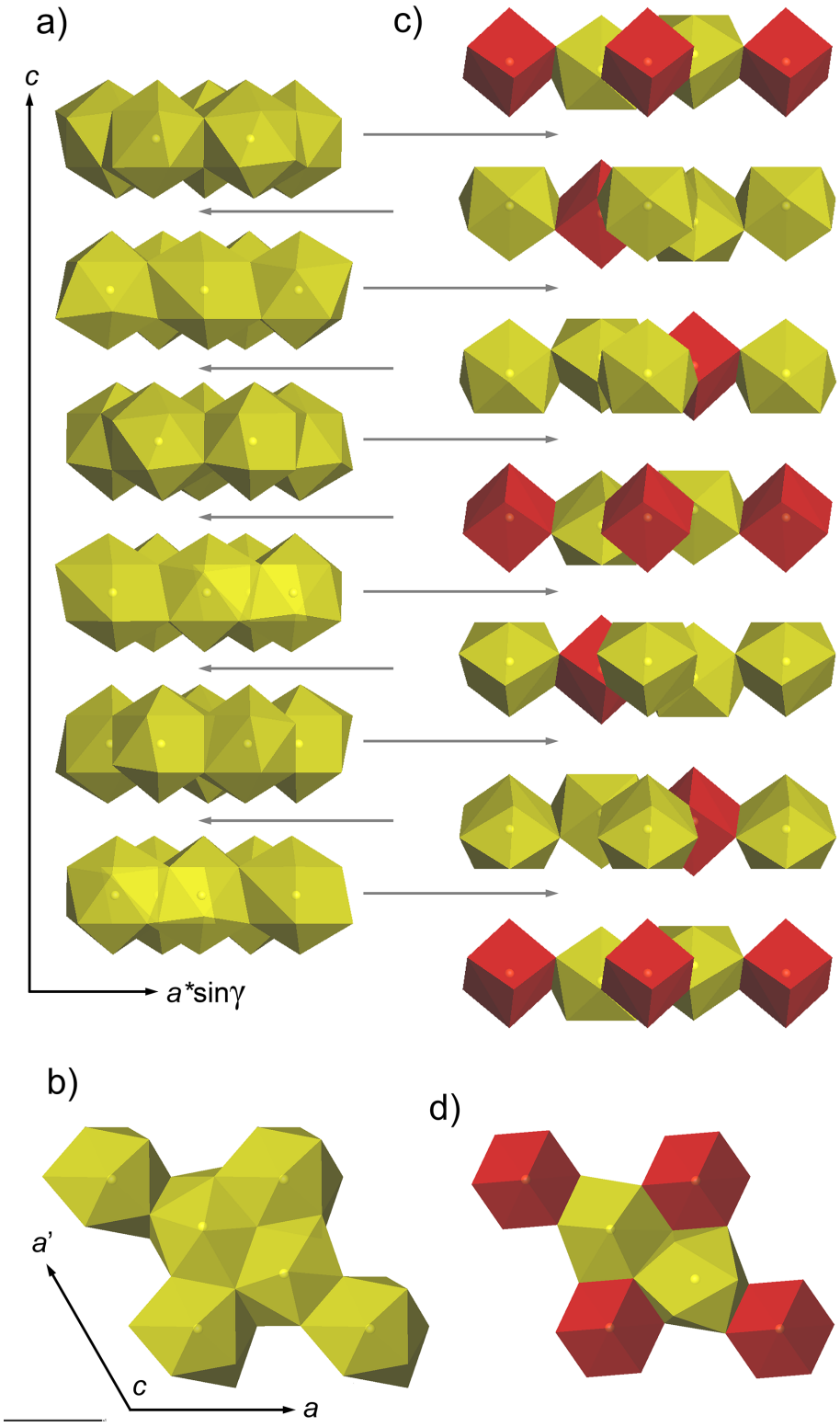

Fig. 6 Crystal structure of perryite: an alternation of layers of two different types along the c-axis. **a,b** – Layers of edge- and face-sharing polyhedra [$SiNi_{12}$]; projections onto (110) and (001) plane, respectively. **c,d** – Layers composed of polyhedra [$SiNi_{10}$] (yellow) sharing common edges with distorted cubes [PNi_8] (red); the same projections as in **a,b**. Drawn using Atoms v.6 (Dowty 2013).

available online at the Journal web site (http://dx.doi.org/10.3190/jgeosci.331).

References

Barbaro A, Domeneghetti MC, Litasov KD, Ferrière L, Pittarello L, Christ O, Lorenzon S, Alvaro M, Nestola F (2021) Origin of micrometer-sized impact diamonds in ureilites by catalytic growth involving Fe-Ni-silicide: The example of Kenna meteorite. Geochim Cosmochim Acta 309: 286–298

Britvin SN, Dolivo-Dobrovolsky DV, Krzhizhanovskaya MG (2017) Software for processing the X-ray powder diffraction data obtained from the curved image plate detector of Rigaku RAXIS Rapid II diffractometer. Zap Ross Mineral Obsh 146: 104–107 (in Russian)

Britvin SN, Murashko MN, Vapnik Y, Polekhovsky YS, Krivovichev SV, Krzhizhanovskaya MG, Vereshchagin OS, Shilovskikh VV, Vlasenko NS (2020) Transjordanite, Ni_2P, a new terrestrial and meteoritic phosphide, and natural solid solutions barringerite-transjordanite (hexagonal Fe_2P–Ni_2P). Amer Miner 105: 428–436

Britvin SN, Krzhizhanovskaya MG, Zolotarev AA, Gorelova LA, Obolonskaya EV, Vlasenko NS, Shilovskikh VV, Murashko MN (2021) Crystal chemistry of schreibersite, $(Fe,Ni)_3P$. Amer Miner 106: 1520–1529

Britvin SN, Murashko MN, Krzhizhanovskaya MG, Vereshchagin OS, Vapnik Ye, Shilovskikh VV, Lozhkin MS, Obolonskaya EV (2022) Nazarovite, $Ni_{12}P_5$, a new terrestrial and meteoritic mineral structurally related to nickelphosphide, Ni_3P. Amer Miner: DOI 10.2138/am-2022-8219

Casanova I, Keil K, Newsom HE (1993) Composition of metal in aubrites: Constraints on core formation. Geochim Cosmochim Acta 57: 675–682

Dolomanov OV, Bourhis LJ, Gildea RJ, Howard JAK, Puschmann H (2009) OLEX2; a complete structure solution, refinement and analysis program. J Appl Crystalogr 42: 339–341

Dowty E (2013) ATOMS v.6. A computer program for displaying atomic structures. Shape software, Kingsport, TN

Drábek M (2006) Phosphide solid-solutions within the metal-rich portion of the quaternary system Co–Fe–Ni–P AT 800 °C. Canad Mineral 44: 399–408

Ellner M, Heinrich S, Bhargava M, Schubert K (1979) Einige strukturelle untersuchungen in der mischung $NiSi_N$. J Less-Common Met 66: 163–173

Flack HD, Bernardinelli G (2008) Applications and properties of the Bijvoet intensity ratio. Acta Crystallogr A64: 484–493

Frank K, Schubert K (1971) Kristallstruktur von $Ni_{31}Si_{12}$. Acta Crystallogr B27: 916–920

Fredriksson K, Henderson EP (1965) The Horse Creek, Baca County, Colorado, iron meteorite. Trans Amer Geophys Un 46: 121

Garvie LAJ, Ma C, Ray S, Domanik K, Wittmann A, Wadhwa M (2021) Carletonmooreite, Ni_3Si, a new silicide from the Norton County, aubrite meteorite. Amer Miner, DOI 10.2138/am-2021-7645

Grokhovskii VI, Ivanov AV (1986) Graphite-perryite segregation in Kaidun III kamacite. Meteoritika 45: 20–22 (in Russian)

Il'nitskaya ON, Aksel'rud LG, Mikhalenko SI, Kuz'ma YuB (1987) Crystal structure of alpha-Ni_8P_3. Kristallografija 32: 50–54 (in Russian)

Keil K (1968) Mineralogical and chemical relationships among enstatite chondrites. J Geophys Res 73: 6945–6976

Kimura M, Lin Y (1999) Petrological and mineralogical study of enstatite chondrites with reference to their thermal histories. Antarct Meteori Res 12: 1–18

Larsson E (1965) An X-ray investigation of the Ni–P system and the crystal structures of NiP and NiP_2. Ark Kemi 23: 335–365

Lee MR, Russell SS, Arden JW, Pillinger CT (1995) Nierite (Si_3N_4), a new mineral from ordinary and enstatite chondrites. Meteoritics 30: 387–398

Lin Y, El Goresy A (2002) A comparative study of opaque phases in Qingzhen (EH3) and MAC 88136 (EL3): representatives of EH and EL parent bodies. Meteorit Planet Sci 37: 577–599

Macrae CF, Edgington PR, McCabe P, Pidcock E, Shields GP, Taylor R, Towler M, van de Streek J (2006) Mercury: visualization and analysis of crystal structures. J Appl Crystallogr 39: 453–457

Marsh RE (1994) The centrosymmetric – noncentrosymmetric ambiguity: some more examples. Acta Crystallogr A50: 450–455

McCall GJH (1965) A meteorite of unique type from Western Australia: The Mount Egerton stony-iron. Mineral Mag 35: 241–249

Meteoritical Bulletin Database. Accessed on June 15, 2021, at https://www.lpi.usra.edu/meteor/metbull.php?code=16774

Nagahara H, El Goresy A (1984) Yamato-74370: a new enstatite chondrite (EH4). Lunar Planet Sci XV: Abstr 583

Nehru CE, Prinz M, Weisberg MK, Delaney JS (1984) Parsa: an unequilibrated enstatite chondrite (UEC) with an aubrite-like impact melt clast. Lunar Planet Sci Conf, XV: Abstr 597

Okada A, Keil K, Taylor GJ, Newsom H (1988) Igneous history of the aubrite parent asteroid: Evidence from the Norton County enstatite chondrite. Meteoritics 23: 59–74

Okada A, Kobayashi K, Ito T, Sakurai T (1991) Structure of synthetic perryite, $(Ni,Fe)_8(Si,P)_3$. Acta Crystallogr C47: 1358–1361

Prinz M, Nehru CE, Weisberg MK, Delaney JS (1984) Type 3 enstatite chondrites: a newly recognized group of unequilibrated enstatite chondrites (UEC'S). Lunar Planet Sci Conf, XV: Abstr 653

Rambaldi ER, Rajan RS (1983) Chemical and textural study of Qingzhen, a highly unequilibrated enstatite chondrite. Lunar Planet Sci Conf, XIV: Abstr 626

Ramdohr P (1963) The opaque minerals in stony meteorites. J Geophys Res 68: 2011–2036

Reed SJB (1968) Perryite in the Kota-Kota and South Oman enstatite chondrites. Mineral Mag 36: 850–854

Sheldrick GM (2015) Crystal structure refinement with SHELXL. Acta Crystallogr C71: 3–8

Skála R, Císařová I (2005) Crystal structure of meteoritic schreibersites: determination of absolute structure. Phys Chem Miner 31: 721–732

Wai CM (1970) Metal phase of Horse Creek, Mount Egerton, and Norton County enstatitic meteorites. Mineral Mag 37: 905–908

Wasson JT, Wai CM (1970) Composition of the metal, schreibersite and perryite of enstatite achondrites and the origin of enstatite chondrites and achondrites. Geochim Cosmochim Acta 34: 169–184

Westrip SP (2010) publCIF: software for editing, validating and formatting crystallographic information files. J Appl Crystallogr 43: 920–925

Yang J, Wu X, Qin S (2015) p-V equation of state of $(Fe_{0.03}Ni_{0.97})_8$ $(Si_{0.79}P_{0.21})_3$. Chin J High Press Phys 25: 275–280

Zhang P, Ji S-J, Zhang D, Xue H-G, Suen N-T (2021) Synthesis, Crystal Structure, Electronic Structure, and Electrocatalytic Hydrogen Evolution Reaction of Synthetic Perryite. Inorg Chem 60: 3006–3014